PCCP

Accepted Manuscript

ROYAL SOCIETY OF CHEMISTRY

www.rsc.org/pccp

Revealing photofragmentation dynamics through interactions between Rydberg states: REMPI of HI as a case study

Helgi Rafn Hróðmarsson and Ágúst Kvaran*
Science Institute, University of Iceland, Dunhagi 3, 107 Reykjavík, Iceland.

*Correspondence should be addressed to:

AgustKvaran
Permanent address:
Science Institute,
University of Iceland,
Dunhagi 3, 107 Reykjavík,
Iceland
Phone: +354-525-4672 (A.K. office)
Phone: +354-525-4800 (main office)
Fax: +354-552-8911 (main office)
E-mail: agust@hi.is

Abstract

High energy regions of molecular electronic states are largely characterized by the nature and involvement of Rydberg states. Whereas the number of observed dynamical processes that are due to interactions between Rydberg and valence states, reports on corresponding effect of Rydberg-Rydberg state interaction, in the literature are scarce. Here we report a detailed characterization of the effects of interactions between two Rydberg states on photofragmentation processes, for a hydrogen halide molecule. Perturbation effects, showing as rotational line shifts, intensity alterations and line-broadenings in REMPI spectra of HI, for two-photon resonance excitations to the $j^3\Sigma^-(0^+;\ v' = 0)$ and $k^3\Pi_1(v' = 2)$ Rydberg states, are analyzed. The data reveal pathways of further photofragmentation processes involving photodissociation, autoionization and photoionization affected by the Rydberg-Rydberg state interactions as well as the involvement of other states, close in energy. Detailed mechanisms of the involved processes are proposed.

INTRODUCTION

Since the original work on the spectroscopy of the hydrogen halides, performed by Price,[1] hydrogen iodide (HI) has been the subject of various studies related to its electronic structure, potential energy surfaces, photodissociation and photofragmentations. Absorption measurements performed by Tilford et al.,[2] M. L. Ginter et al.,[3] and D. S. Ginter et al.[4], respectfully, provided a comprehensive overview of Rydberg and valence (ion-pair) states observed in the excitation region between 52 610 cm^{-1} and 74 400 cm^{-1}. Assignments of the HI Rydberg states were based on comparison of the observed spectral series and known Rydberg series for xenon.[5] Lower energy states, of repulsive potential curves, in the range 32 000 cm^{-1} to 52 000 cm^{-1}, as well as relevant photodissociation branching ratios have been studied extensively [6-22] and a number of ab initio calculations of the relevant potential curves have been performed.[23-30] Studies of competitions between spin-orbit autoionization and predissociation of Rydberg states have been performed[25, 31-33] and the ground state of the

molecular ion, HI^+, has been explored by a number of experimental techniques.[27, 34-42] The first resonance enhanced multiphoton ionization (REMPI) experiments for HI were performed by Wright & McDonald[43] and Pratt & Ginter.[44] Later, the REMPI technique was used complementarily with photolysis for three-photon excitations in the region of 82 050 cm^{-1} and 83 250 cm^{-1},[45] and branching ratios were determined by previous usage of the photolysis technique.[14, 19, 21, 22, 29] Velocity map images, following a three-photon excitation scheme at 108 000 cm^{-1} (13.39 eV) and 125 700 cm^{-1} (15.59 eV) were recorded by Loock et al.[46], where iodine fragments were used to derive information regarding interactions between repulsive and superexcited states. Two-dimensional photoelectron spectroscopy studies of HI were performed for the 89 530 – 119 800 cm^{-1} (11.10 – 14.85 eV) excitation region by Hikosaka & Mitsuke,[47] to cover the energy range between the ionic ground state ($X^2\Pi$) and the excited ionic state $A^2\Sigma^+$. In recent years, an appreciable amount of REMPI work has been performed on the hydrogen halides, emphasizing interactions between Rydberg and ion-pair states, mostly for HCl[48-51] and HBr.[51, 52] The emphasis has, only recently, shifted towards HI for the two-photon excitation region of 69 600 – 73 500 cm^{-1}, where relevant studies have focused on the assignment of new states,[53] state interactions[54] as well as identifications and assignments of hidden (or dark) states.[55]

Localized level-to-level interactions between Rydberg states and ion-pair states have been investigated to a large extent for the hydrogen halides both qualitatively and quantitatively, whereas analogous interactions between Rydberg states have only been dealt with speculatively. (e.g. see Ref. 55 and references therein). In this paper we present, for the first time, a characterization of localized level-to-level interactions between two Rydberg states in one of the hydrogen halide molecules (HI). Based on perturbation effects in the REMPI spectra of HI for two-photon resonance excitations to the triplet Rydberg states $j^3\Sigma^-$ (0^+; $v' = 0$) and $k^3\Pi_1(v' = 2)$, state interactions are determined quantitatively. Furthermore, the

impact of the state interactions on photofragmentation pathways upon additional photoexcitation is explored.

EXPERIMENTAL

The experimental apparatus as well as relevant equipment parameters are similar to that described in previous publications.[52-55] Therefore, only a short summary will be addressed.

Mass resolved REMPI data for a HI molecular beam were recorded. The beam was created by a jet expansion of a pure gas sample through a pulsed nozzle and ions were directed into a time-of-flight tube and detected by a microchannel plates (MCP) to record the ion yields as a function of mass and laser radiation wavenumber. Signals were recorded by a LeCroy Wavesurfer 44MXs-A, 400 MHz storage oscilloscope. Tunable excitation radiation was generated by an Excimer laser-pumped dye laser system, using a Lambda Physik COMPex 205 Excimer laser and a Coherent ScanMatePro dye laser, with a C-540 dye. Frequency doubling was achieved by using a SIRAH second harmonic generator (SHG). Laser power was minimized to prevent saturation effects and power broadening. Laser calibration was based on observed (2 + 1) REMPI iodine atomic lines.[55] The accuracy of the calibration was found to be about ± 0.5 cm^{-1} on the laser wavenumber scale, hence about ± 1.0 cm^{-1} on the two-photon wavenumber scale.

THEORY

Line shift determining factors

In molecular spectra, perturbations give invaluable insight into the mechanisms of various state interactions. State interactions are classified as homogeneous ($\Delta\Omega = 0$) and heterogeneous ($\Delta\Omega \neq 0$) and the resulting perturbations differ in accordance with their nature. Thus, if $\Delta\Omega = 0$, the interactions are independent of rotational quantum numbers, J', whereas

if $\Delta\Omega \neq 0$, interactions are J' dependent. In REMPI spectra of the hydrogen halides, these effects have been found to manifest themselves as spectral line shifts (hence energy level shifts) in the cases of interactions between Rydberg and ion-pair states. [48-50, 52, 54-57]

When dealing with perturbations, caused by two interacting states, (1) and (2), it is customary to utilize the diagonalization of the Hamiltonian matrix elements[58] for interactions between energy levels with the same J' quantum numbers, which depend on the zeroth order unperturbed energies ($E_{J'}{}^0(1)$ and $E_{J'}{}^0(2)$) and the interaction strength (W_{12}),

$$\begin{array}{ccc} & 1 & 2 \\ 1 & E_{J'}^0(1) & W_{12} \\ 2 & W_{12} & E_{J'}^0(2) \end{array} \qquad (1)$$

for

$$E_{J'}^0(i) = \nu^0(i) + B'(i)J'(J'+1) - D'(i)J'^2(J'+1)^2\,, i = 1,2 \qquad (2)$$

where $\nu^0(i)$ are the band origins, $B'(i)$ are the rotational constants, and $D'(i)$ are the centrifugal distortion constants. This yields the observed, perturbed energy levels ($E_{J'}(1)$ and $E_{J'}(2)$),

$$E_{J'}(i) = \frac{1}{2}\left(E_{J'}^0(1) + E_{J'}^0(2)\right) \pm \frac{1}{2}[4|W_{12}|^2 + (E_{J'}^0(1) - E_{J'}^2(2))]^{1/2}, i = 1,2 \qquad (3)$$

For homogeneous interactions, W_{12} is a constant, whereas for heterogeneous interactions

$$W_{12} = W'_{12}\sqrt{\left(J'(J'+1)\right)} \qquad (4)$$

where W'_{12} is a constant.

In the limit of $\Delta E_{J'}$ (= $E_{J'}(1)$ - $E_{J'}(2)$) ≈ 0, solutions are approximated by the degenerate state perturbation theory[58, 59] which yields very large energy level shifts, characteristic for "near-degenerate" J' levels. Hereby, we shall refer to such cases as "near-degenerate interactions" to distinguish them from "non-degenerate interactions".

Line strength determining factors

Several factors govern the rotational line strengths in REMPI spectra. The relative intensities (I_{rel}) are proportional to the product of the cross sections of the resonance excitation step (σ_1) and the photoionization (σ_2).

$$I_{rel} \propto \sigma_1 \sigma_2 \quad (5)$$

The cross section for the photoionization step (σ_2), is commonly a slowly varying function with photon energy and in the cases where the excitation frequency range is narrow, it can be assumed to be constant, of a value depending on the ionized state (σ_2 (Ω')). The cross section of the resonance excitation step (σ_1) is expressed as, [60-62]

$$\sigma_1 \sim \left| \sum_i \frac{\langle 1|\boldsymbol{\varepsilon}\cdot\boldsymbol{\mu}|i\rangle\langle i|\boldsymbol{\varepsilon}\cdot\boldsymbol{\mu}|0\rangle}{\Delta E_{0i} - h\nu + C(\Gamma_i)} \right|^2 \quad (6)$$

for a two-photon transition between the states $|0\rangle$ and $|1\rangle$. $h\nu$, is the photon energy, $\boldsymbol{\varepsilon}\cdot\boldsymbol{\mu}$ is the operator representing the interaction between the electric field component of the electromagnetic wave and the molecular charge dipole and $|i\rangle$ is an intermediate state with energy ΔE_{0i}. Based on the Born-Oppenheimer approximation, Eq. (6) can be simplified and approached by a product of terms depending on the electron configuration (C_e) and the nuclear motions ($S(\Delta\Omega, J', J'')$ and $FCF(v', v'')$),

$$\sigma_1 = C_e \, S(\Delta\Omega, J', J'') \, FCF(v', v'') \quad (7)$$

where $FCF(v', v'')$ is the Franck-Condon-Factor, depending on the vibrational quantum numbers v' and v'' and $S(\Delta\Omega, J', J'')$ is the transition strength, depending on the rotational quantum numbers (J', J'') and the difference in the total electronic angular momentum quantum numbers ($\Delta\Omega = |\Omega' - \Omega''|$). $S(\Delta\Omega, J', J'')$ also depends on the parallel ($\mu_\parallel$) and perpendicular ($\mu_\perp$) transition dipole moments that correspond to transitions to the virtual intermediary state(s), $|i\rangle$.

$$\mu_{||} = \langle \Omega | \boldsymbol{\varepsilon}\cdot\boldsymbol{\mu} | \Omega \rangle \quad (8a)$$

$$\mu_{\perp} = \langle \Omega \pm 1 | \boldsymbol{\varepsilon}\cdot\boldsymbol{\mu} | \Omega \rangle \quad (8b)$$

The general expression of the two-photon transition strength is[63]

$$S(\Delta\Omega, J', J'') = s_0\mu_0^2 + s_2\mu_2^2 \quad (8c)$$

where s_0 and s_2 are functions of J' and J'' as well as Ω' and Ω'' and are written in terms of Clebsch-Gordan coefficients for zeroth order coefficients (subscript 0) and second order coefficients (subscript 2).[63, 64] μ_0^2 and μ_2^2 are sum and product functions of ($\mu_\parallel$) and ($\mu_\perp$) which collectively represent the effect of all one-photon transition moments that give rise to parallel and perpendicular transitions.

Furthermore, the relative intensity (I_{rel}) is proportional to the population ($N(v'', J'')$) and the degeneracy ($g(J'')$) of the absorbing state as well as the laser power (P) as P^n, where n represents the total number of photon absorbed.[65]

All in all, I_{rel} can be expressed as

$$I_{rel} = K(\Omega')\, P^n [C_e S(\Delta\Omega, J', J'') FCF(v', v'')]\, [g(J'')N(v'', J'')] \quad (9)$$

where $K(\Omega')$ is a constant depending on the ionized state. For a certain electronic and vibrational ($v' \leftarrow\leftarrow v''$) transition C_e and $FCF(v', v')$ can be assumed to be constant, to a first approximation.

Line width determining factors

Lower limit lifetimes (τ_{min}) can be derived from spectral line widths (Γ) by[58]

$$\tau_{min}(ps) = 5.3/\Gamma(cm^{-1}) \quad (10)$$

Line widths of Rydberg state spectra are primarily affected by predissociation processes. Such processes can occur via gateway Rydberg states in which cases the lifetimes, hence line-widths, depend on bound-to-bound Rydberg state interactions as well.[52, 54, 55]

RESULTS

Spectral observations

Fig. 1 shows REMPI spectra in the two-photon excitation region of 73 098 – 73 261 cm^{-1}. By comparison with the work by Ginter et al.[4] the major spectral features were assigned to two-photon resonance transitions to the $j^3\Sigma^-(0^+;\ v' = 0)$ and $k^3\Pi_1(v' = 2)$ Rydberg states with the electron configurations $(\sigma^2\pi^3)5d\pi$ and $(\sigma^2\pi^3)5d\delta$, respectively. In this respect, it should be mentioned that, whereas, the lighter hydrogen halides have been assigned according to the Hunds case (a) and Hunds case (b) classifications, HI correlates better with the Hunds case (c) classification[2-4, 55] and, furthermore, that superexcited states of HI have been shown to display the Hunds case (e) characteristics.[25] Nevertheless, it has been a convention to retain the assignments of HI states according to the Hunds cases (a) and (b).[2-4, 43-45, 54, 55, 57, 65, 66] The observed line positions (Fig. 1) of the $j(0)$ (i.e. $j^3\Sigma^-(0^+;\ v' = 0)$) and $k(2)$ (i.e. $k^3\Pi_1(v' = 2)$) spectra are presented in Table 1. It is clear that level-to-level interactions are taking place for $J' = 9 - 10$. Thus, the corresponding $j(0)$ lines are found to be significantly spread apart, whereas the $J' = 9$ and 10 lines for the $k(2)$ spectrum are interchanged. The $J' = 10$ line of the $k(2)$ spectrum is shifted upwards in energy, so radically, that it merges with the $J' = 8$ peak. The assignment was adequately reproduced by simulation calculations by use of the PGOPHER program.[67] Analogous effects have been observed in REMPI spectra of hydrogen halides in the cases of Rydberg to ion-pair interactions.[50-52, 54, 55, 57] The quantum energy levels of the $j(0)$ and $k(2)$ states, derived from the spectra, are presented in Fig. 2. These imply near degenerate interactions between the $j(0)$ and $k(2)$ Rydberg states for $J' = 9 - 10$, which appear as an expansion of the energy level gap for $k(2)$ but a compression of the corresponding levels for $j(0)$. The symmetries of the two Rydberg states suggest that the interaction of concern is L-uncoupling ($\Delta S = 0$, $\Delta\Omega = \pm 1$), i.e. a gyroscopic perturbation.[58] In addition to line-shift analysis, the REMPI spectra were explored in terms of signal intensities, and linewidths alterations(see below).

In the region between about 73 196 cm^{-1} and 73 210 cm^{-1} weak signals are found in all the spectra. These could not be assigned to either the $j(0)$ or the $k(2)$ state. At 73 117.9 cm^{-1} a strong iodine atomic line is observed. It is a (2 + 1) REMPI of I [$^2P_{1/2}$] for resonance excitation to the atomic Rydberg state $^2[1]°_{1/2}$ ($5s^25p^4(^3P_2)9p$).[68] Furthermore, weak signals close to 73 110 cm^{-1}, are due to transition to the $V(m + 12)$ (i.e. $V^1\Sigma^+(v' = m + 12)$) ion-pair state. [55] Few weak peaks in the region 73 100 – 73 115 cm^{-1} remain unassigned. These, most likely, belong to the R and/or S series of the $P(0)$ ($P^1\Delta_2(v' = 0)$) Rydberg state spectrum or possibly high J's of the $V(m + 13)$ ion-pair state.[55] A weak signal observed at 73 200 cm^{-1} is attributed to a transition to a previously unobserved $^3\Sigma^-$ ($\Omega = 1$) Rydberg state (see discussion below).

Perturbation analysis

A two-state deperturbation analysis was performed for the $j(0)$ and $k(2)$ Rydberg states. It produced the interaction strengths and spectroscopic constants presented in Table 2 and Table 3, respectively. A more detailed discussion of the perturbation analyses procedures follows.

Line shift (LS)-effects

To a first approximation the energy spacing between adjacent rotational levels ($\Delta E_{J',J'-1} = E(J') - E(J' - 1)$) of a non-interacting Rydberg state will display linear behavior as a function of J'. The slope equals $2B_{v'}$, where $B_{v'}$ is the v'-dependent rotational constant. Deviations from linearity are indications of perturbation effects due to state interactions, where rotational levels experience level-to-level repulsions for states with same J' quantum numbers. This effect can be seen more clearly by plotting the difference between the observed level energies ($E_{J'}$), derived from the rotational lines, and the corresponding zeroth order

energies derived from Eq. (2) (i.e. "reduced term value plots"). This has been referred to as line shift (LS)-effects.[54, 55]

LS-effects are clearly apparent in the $j(0)$ and $k(2)$ spectra, as mentioned before. Respective rotational energy level differences, as a function of J', are presented in Fig. 3(a) along with the corresponding deperturbed curves. The $j(0)$ state displays slight increases in the energy gaps between $J' = 7$ and $J' = 8$ ($\Delta E_{8,7}$) and between $J' = 8$ and $J' = 9$ ($\Delta E_{9,8}$), followed by a significant decrease in the energy gap between $J' = 9$ and $J' = 10$ ($\Delta E_{10,9}$). This effect is "mirrored" in the plot for the $k(2)$ state, which shows significant decreases in $\Delta E_{9,8}$ and $\Delta E_{9,8,}$ but an increase in $\Delta E_{10,9}$. It is worth noting that, whereas, the $j(0)$ state is experiencing a significant increase in $\Delta E_{8,7}$ the corresponding decrease in $\Delta E_{8,7}$ for the $k(2)$ state is less. The reduced term value plots shown in Fig. 3(b) show the LS-effects even clearer. Therein, the $k(2)$ state levels are experiencing slight repulsion effects, downwards, for $J' = 8$ and 9 but a strong repulsion, upwards, for $J' = 10$. This effect is virtually "mirrored" in the $j(0)$ state. In addition, the $j(0)$ state, displays upward shifts of levels $J' = 3$ - 6, followed by a slight tug downward for $J' = 7$. The additional "non-mirror" effects observed for the $j(0)$ state suggests an additional interaction with another (hidden) state.[55] This will be discussed in more detail below. Furthermore, according to the reduced term value plot (Fig. 3(b)), levels J' = 11 and 12 of the $k(2)$ state display upward repulsion effects.

Line intensity (LI)-effects

The REMPI data for resonance excitations to a Rydberg state of the hydrogen halides (HX) can consists of ion signals from the parent molecule (HX^+) as well as the ionic fragments (X^+ and H^+). The integrated signals of each respective ion reveal the relative fractions of the various formation pathways, which can depend on state interactions.[48-52, 54, 55] This has been referred to as line intensity (LI) -effects.[54, 55] Thus, in cases of interactions

between Rydberg and ion-pair states, the presence of a J' dependent halogen ion signal (X^+) in the REMPI spectrum of a Rydberg state is found to be a strong indication of a Rydberg to ion-pair state mixing.[48, 69-72] The intensity ratio, $I[X^+]/I[HX^+]$, (and to a lesser extent $I[H^+]/I[HX^+]$) has been applied to a number of interacting systems to evaluate the level of state mixing.[50, 52, 54, 55, 57] Analysis based on LI-effects for Rydberg to Rydberg state interactions, as seen here for the $k(2)$ and $j(0)$ Rydberg states, on the other hand, have not been developed and require a different approach.

According to Eq. (9), the intensity ratio of the Q rotational lines, of same J', for the $k(2)$ ($\Omega' = 1$) and $j(0)$ ($\Omega' = 0^+$) spectra (i.e. $I(k)/I(j)$), in the case of no interaction, simplifies to,

$$\frac{I_{rel}[k,J]}{I_{rel}[j,J]} = \frac{K(k)\,S(k)}{K(j)\,S(j)} \qquad (11a)$$

where $K(k)$ and $K(j)$ are constants for the two states with values depending on the corresponding ionization cross sections. $S(k)$ and $S(j)$ are the corresponding transition strengths. By using J' -dependent expressions for s_0 and s_2 to determine $S(k)$ ($\Delta\Omega = 1$) and $S(j)$ ($\Delta\Omega = 0$) (Eq. 8)[60, 63, 73] Eq. (11a) takes the form,

$$\frac{I_{rel}[k,J]}{I_{rel}[j,J]} = \frac{K(k)}{K(j)} \frac{\left(\frac{1}{10(2J+3)(2J-1)}\right)}{\left(\mu_0^2\left(\frac{1}{9}(2J+1)\right)+\mu_2^2\left(\frac{1\ \ (J+1)(J+2)}{45(2J+3)(2J-1)}\right)\right)} \qquad (11b)$$

for $J = J' = J''$. An investigation of the rotational line intensities of the $j(0)$ and $k(2)$ spectra (Fig. 1 and Fig. 4 (a)) shows that the total ion intensities of the $k(2)$ spectrum are relatively large for high J's, whereas the opposite is found for the $j(0)$ spectrum. The corresponding intensity ratio ($I_{rel}(k(2)/I_{rel}(j(0))$, as a function of J' (Fig. 4(b)) shows close to constant value for low J's but large increases for high J's. The data points for low J's ($J' = 2 - 5$), where interaction between the two states is found to be negligible (see previous section), were fitted by the expression on the right side of Eq. (11b), for μ_0^2, μ_2^2 and $K(k)/K(j)$ as variables. This

gave a smooth, slightly varying function of J' for all J's (Fig. 4(b)). The discrepancy between the data points and the fit curve is a clear indication of state mixing / interaction for high J's (J'= 8 – 10 in particular), which can be partly due to a change in the transition strength (S) and partly because of changes in the ionization cross sections (hence the K's) which manifest as enhanced intensities for high J's in the case of the k(2) spectrum, but as lowered intensities for the j(0) spectrum. This can be referred to as "intensity borrowing".

A closer look at the H^+ signals for the k(2) and j(0) spectra (Fig. 5 (a)) reveals that the j(0) spectrum shows a distinctly greater propensity for H^+ formation compared to the k(2) spectrum, for low J's. For higher J's ($J' > 7$), on the other hand, the relative H^+ intensity for j(0) decreases slightly, but significantly, whereas, for k(2), it increases. This observation further supports the effect of "intensity borrowing", given that the j(0) state yields a greater amount of H^+ ions (Fig. 1).

The relative contributions of the I^+ and HI^+ ion signals as a function of J' for the j(0) spectrum are shown in Fig. 5(b). The curves show clear "mirror image effects"; where relative increases of the I^+ signal is in tandem with a decrease of the HI^+ signal and vice versa. No such effect is observed in the k(2) spectrum. As previously stated, a rise in the intensity of a halogen fragment ion signal and a decrease in that of the molecular ion for a Rydberg state is characteristic of increased interactions with an ion-pair state. We believe that this effect can, partly, be attributed to additional non-degenerate interactions with ion-pair vibrational state(s). The sharp change in the relative intensities for J'= 6 - 7, on the other hand, suggests that near-degenerate interactions also are involved.

Line width (LW)-effects

The line-widths of all the ion signals for the j(0) and k(2) spectra as a function of J' are presented in Figs. 6(a) and 6(b), respectively. For j(0) the line-widths, are small (ca. 0.2 cm^{-1})

and close to constant for low J's ($J' = 0 – 5$), show slight increase for $J' = 6$ - 7, drop in the value for $J' = 8$ and finally a relatively large increase for $J' = 9$. The line-widths for the $k(2)$ spectral peaks also are low in values and close to constant, within experimental error, for low J's ($J' = 2 – 8$) as well as for $J' = 10$, whereas a severe line broadening is observed for $J' = 9$ as well as for $J' = 10$ and 11.

DISCUSSION

Additional perturbing or hidden states

The perturbation analyses, mentioned above, revealed several features in the REMPI spectra that could not be explained by near-degenerate interactions between the $j(0)$ and the $k(2)$ states. These are, in all likelihood, a direct result of interactions with other states, close in energy which may be either hidden or not hidden.[55]

$^3\Sigma^-(1)$ state: A number of observations in the $j(0)$ spectrum, mentioned above, suggest that the $j^3\Sigma^-(0^+;\ v' = 0)$ state is interacting with an unknown (hidden) state. Thus, dips observed in the reduced term value plot for $J' = 7$ (Fig. 3(b)), increases in relative I^+ signals and corresponding decreases in relative HI^+ signals (Fig. 5(b)) as well as line-width alterations (Fig. 6(a)) for $J' = 6 – 7$ are all indicative of weak, near-degenerate interaction for $J' = 6 – 7$. A candidate for such a weak perturber, which apparently is not affecting the, close in energy, $k^3\Pi_1(v' = 2)$ state is a state which will satisfy the requirements of being (i) -a triplet state ($\Delta\Sigma = 0$), (ii) – a Σ state, (iii) – a state of minus parity "-"and iv) an $\Omega = 1$ state, i.e. a $^3\Sigma^-$ (1) state. Based on the energetics of known or predicted Rydberg states for HI[53] we suggest that this could either be the $g^3\Sigma^-(1)$ ($v' = 2$) state with electron configuration $[\sigma^2\pi^3]6p\pi$ or the $q^3\Sigma^+(1)$ ($v' = 0$) state with electron configuration $[\sigma^2\pi^3]4f\pi$. Furthermore, the weak unassigned spectral features, unclear in structure, which is observed between the Q rotational lines for J'

= 6 and 7 of the $j(0)$ spectrum (see above and Fig. 1) we assign to the Q lines of the corresponding spectrum.

Ion-pair states: The following observations of the $k(2)$ spectrum, all suggest that the $k(2)$ state is interacting with an additional state. Increases in rotational energies (Fig. 3 (b)), relative intensity of the H^+ signals (Fig. 5(a)) and line broadenings (Fig.6(b)), observed for $J' = 11 - 12$, are all indicative of weak near-degenerate interactions. Whereas, rotational lines for the ion-pair state $V^1\Sigma^+(v' = m + 13)$ for $J' > 8$ have not been observed in REMPI[55] extrapolation of low rotational energy levels to $J' > 8$ reveals that levels $J' = 11$ and 12 are only slightly lower in energy than the corresponding levels of the $k(2)$ state and could be the cause of the observed perturbation effects. Furthermore, absorption spectra[4] ***s***uggest that levels higher than $J' = 7$ of $V(m + 13)$ are, indeed, mixed.

Photofragmentations

The two-photon scan region that spans the rotational line spectra of the $k(2)$ and $j(0)$ states of about 73 100 – 73 260 cm^{-1} (Fig. 1) corresponds to a three-photon excitation region of 109 650 – 109 890 cm^{-1} (see Fig. 7). This excitation region has been explored in number of studies by various techniques.[35-38, 41, 45, 47] It is above the molecular ion ground states, $X^2\Pi(\Omega = 1/2, 3/2)$, which correlate with $H(n = 1) + I^+(^3P_2)$ and below the first excited bound ionic state, $A^2\Sigma^+$, which correlates with $H(n = 1) + I^+*(^1D_2)$. Furthermore, a superexcited state ($HI^{\#}$), which belongs to a Rydberg series that converges to the $A^2\Sigma^+$ state ($[A^2\Sigma^+]5d\pi$), is believed to be found in that region and is likely to play an important role in further ionization processes.[31, 35, 47]

Velocity map imaging studies coupled with REMPI by Regan et al.[45] for four-photon excitation into this region revealed two major H^+ formation mechanisms. The first mechanism (i) involves the formation of $H^*(n = 2) + I(3/2)$, followed by one-photon ionization of $H^*(n =$

2). The second mechanism (ii) involved the formation of high vibrational levels ($v^+ \geq 15$) of the HI^+ $X^2\Pi$ state followed by one-photon photodissociation via the $^2\Pi_{3/2}$ repulsive state to form H^+ + I(3/2). These mechanisms resemble those found to occur in REMPI of HCl[74-77] and HBr.[76, 78, 79] By analogy with observations for HCl[49, 74-76, 80, 81] and HBr[52, 76, 78, 79] I^+ formation is likely to involve two additional mechanisms, i.e., (iii) autoionization of $HI^{\#}$, above the dissociation limit of the ionic states, to form the molecular ion in an unstable state ($HI^+(\varepsilon)/HI^+*(\varepsilon)$) followed by dissociation (see Fig. 7) and (iv) dissociation of $HI^{\#}$ to form iodine in an atomic Rydberg state (I**) followed by photoionization. The significance of the various ion formation mechanisms ((i) – (iv)) depends on the nature of the resonance excited states (HI**(v′, J')) involved. Formation and ionization of the excited atom fragments (H* and I**; (i) and (iv)) preferably will occur for long range excitations as to be expected for ion-pair states or Rydberg states which interact (mix) with ion-pair states. Similarly HI^+/HI^+* species are likely to be formed in high v^+ levels, followed by photodissociation to form H^+ in the cases of long range excitations (from ion-pair states or mixed "Rydberg- ion-pair states"), whereas population of low v^+ levels and small or negligible H^+ formation is more likely to follow short range excitations of pure Rydberg states.

The photoionization product yields, via excitations to the $j(0)$ and $k(2)$ states, are found to be, in descending order as, $I^+ > HI^+ > H^+$(See Figs. 1 and 5). Whereas the intensity ratios of the I^+ and HI^+ signals is comparable for the two resonance states the relative yield of H^+ is significantly stronger for the $j(0)$ state than for the $k(2)$ state for low J's, but vice versa for high J's (see Figs. 1 and 5(a)).

Photofragmentation of the *j*(0) state:

In accordance with theory,[82] the $j^3\Sigma^-(\Omega' = 0^+, v' = 0)$ state will interact homogeneously with the $V^1\Sigma^+$ ion-pair state through a relatively strong spin-orbit (SO) coupling in the form

of non-degenerate level-to-level interactions in addition to the observed near-degenerate interaction with $k(2)$. Therefore, all the ion formation processes ((i) – (iv)), mentioned in the previous section, whether dominating for short-range (a; Rydberg character) or long-range (b; ion-pair character) excitations are effective to an extent which is determined by the state interaction strength. In the light of our spectral observations and discussion above, we propose the following major photofragmentation processes for HI**, following resonance excitation to the $j(0)$ state,

a) - in the case of a dominating V ion-pair state configuration ($\sigma^1\pi^4\sigma^{*1}$) at long-range:

i) $HI^{**}(\sigma^1\pi^4\sigma^{*1}) + h\nu \rightarrow HI^{\#}([\sigma^1\pi^3\sigma^{*1}]\text{Ry-}\pi)$; parallel transition

$HI^{\#}([\sigma^1\pi^4\sigma^{*1}]\text{Ry-}\pi) \rightarrow H^*(n = 2) + I$

$H^*(n = 2) + h\nu \rightarrow \underline{\mathbf{H^+}} + e^-$

ii) $HI^{**}(\sigma^1\pi^4\sigma^{*1}) + h\nu \rightarrow HI^{\#}([\sigma^1\pi^4]5d\pi)$; perpendicular transition

$HI^{\#}([\sigma^1\pi^4]5d\pi) \rightarrow \underline{\mathbf{HI^+(v^+)/HI^+{}^*(v^+)}} + e^-$; high v^+; autoinization

$HI^+(v^+)/HI^+{}^*(v^+) + h\nu \rightarrow \mathbf{H^+} + I$

iii) $HI^{**}(\sigma^1\pi^4\sigma^{*1}) + h\nu \rightarrow HI^{\#}([\sigma^1\pi^4]5d\pi)$; perpendicular transition

$HI^{\#}([\sigma^1\pi^4]5d\pi) \rightarrow HI^+(\varepsilon)/HI^+{}^*(\varepsilon) + e^-$

$HI^+(\varepsilon)/HI^+{}^*(\varepsilon) \rightarrow H + \underline{\mathbf{I^+}}$

iv) $HI^{**}(\sigma^1\pi^4\sigma^{*1}) + h\nu \rightarrow HI^{\#}$

$HI^{\#} \rightarrow H + I^{**}$

$I^{**} + h\nu \rightarrow \underline{\mathbf{I^+}} + e^-$

b) – in the case of a dominating $j(0)$ Rydberg state configuration ($[\sigma^2\pi^3]5d\pi$) at short-range:

ii) $HI^{**}([\sigma^2\pi^3]5d\pi) + h\nu \rightarrow HI^{\#}([\sigma^1\pi^4]5d\pi)$; perpendicular transition

$HI^{\#}([\sigma^1\pi^4]5d\pi) \rightarrow \underline{\mathbf{HI^+(v^+)/HI^+{}^*(v^+)}} + e^-$; low v^+; autoinization

iii) $HI^{**}([\sigma^2\pi^3]5d\pi) + h\nu \rightarrow HI^{\#}([\sigma^1\pi^4]5d\pi)$; perpendicular transition

$HI^{\#}([\sigma^1\pi^4]5d\pi) \rightarrow HI^{+}(\varepsilon)/HI^{+*}(\varepsilon) + e^{-}$

$HI^{+}(\varepsilon)/HI^{+*}(\varepsilon) \rightarrow H + \mathbf{I^{+}}$

Ions that are formed, are highlighted (bold). According to this scheme, the HI^+ and I^+ ions are both formed via long and short range excitations, whereas H^+ ions are only formed via long range excitations.

Photofragmentation of the *k*(2) state:

The $k^3\Pi(\Omega' = 1, v' = 2)$ state interacts weakly with the $V^1\Sigma^+$ ($v' = m + 13$) ion-pair state in the form of heterogeneous, near-degenerate, level-to-level interactions for high J's ($J' = 11 - 12$) (see above), in addition to the observed near-degenerate interaction with $j(0)$ for $J' \sim 8$ - 10. Hence, since the $j(0)$ state interacts relatively strongly with the manifold of ion-pair vibrational states (see above), the $k(2)$ state, effectively, experiences interaction with the V ion-pair state for $J' \sim 8 - 12$, whereas for $J' < 8$ no couplings with the V state are observed. This complies with the observation of a significantly lower H^+ signal seen in the $k(2)$ spectrum for $J' < 8$ compared to that for $J' = 8 - 9$ suggesting that the H^+ ion formation is strongly associated with a long-range (ion-pair character) excitation as in the case of the $j(0)$ excitation (see above). In light of our spectral observations and discussion above we propose the following major photofragmentation processes for HI**, following resonance excitation to the $k(2)$ state,

a) - in the case of a dominating V ion-pair state configuration ($\sigma^1\pi^4\sigma^{*1}$) for high J's ($J' \sim$ 8 – 12) at long-range: Same as for $j(0)$ in the previous section (a(i) – a(iv))

b) – in the case of a dominating $k(2)$ Rydberg state configuration ($[\sigma^2\pi^3]5d\delta$) at short-range ($J' \sim 1 - 7$):

ii) $HI^{**}([\sigma^2\pi^3]5d\delta) + h\nu \rightarrow HI^{\#}([\sigma^1\pi^4]5d\delta)$; perpendicular transition

$HI^{\#}([\sigma^1\pi^4]5d\pi) \rightarrow \underline{\mathbf{HI^+(v^+)/HI^+{*}(v^+)}} + e^-$; low v^+; autoinization

iii) $HI^{**}([\sigma^2\pi^3]5d\delta) + h\nu \rightarrow HI^{\#}([\sigma^1\pi^4]5d\delta)$; perpendicular transition

$HI^{\#}([\sigma^1\pi^4]5d\delta) \rightarrow HI^+(\varepsilon)/HI^+{*}(\varepsilon) + e^-$

$HI^+(\varepsilon)/HI^+{*}(\varepsilon) \rightarrow H + \underline{\mathbf{I^+}}$

SUMMARY AND OUTLOOK

Mass resolved REMPI spectra due to two-photon resonance excitations of HI were recorded in the excitation region of 73 080 cm^{-1} – 73 265 cm^{-1}. The major observed spectral structures were assigned to transitions from the ground molecular state to the $k^3\Pi_1(v' = 2)$ and $j^3\Sigma^-(0^+; v' = 0)$ Rydberg states.[4] Perturbations in the spectral structures, observable as rotational line shifts (LS-effects), line intensity alterations (LI-effects) as well as linewidth alterations (LW-effects), were interpreted and analyzed in terms of near-degenerate level-to-level state interactions. Whereas number of observations and analyses of localized level-to-level interactions between Rydberg states and ion-pair states have been made for the hydrogen halides, this is the first report of a corresponding work in the case of interactions between two Rydberg states. Perturbation effects in the spectra, which could not be attributed to the $k^3\Pi_1(v' = 2)$ - $j^3\Sigma^-(0^+; v' = 0)$ state mixing, were found to be indicative of interactions with- and the presence of- additional states, close in energy. Their appearances (signal intensities) are either very weak or they are hidden from REMPI detection. Thus, based on perturbation effects observed in the $j(v' = 0)$ spectrum, a $^3\Sigma^-(\Omega = 1)$ state, not observed before, with band origin of about 73 200 cm^{-1}, is proposed. Furthermore, effects attributed to interactions between the $k(v' = 2)$ Rydberg state and the $V(v' = m + 13)$ ion- pair states are identified.

The impact of the state interactions on photodissociation and photofragmentation pathways upon additional photoexcitation was also explored. Figs. 8(a) and 8(b) summarize the major processes involved following resonance excitations to the $j(v' = 0)$ and $k(v' = 2)$ states, respectively. The $j(v' = 0)$ state, which experiences homogeneous, non-degenerate interactions with the $V(v' = m + 12)$ and $V(v' = m + 13)$ ion-pair vibrational states, for all J' levels, therefore, will form the ions H^+, I^+ and HI^+ via one-photon excitations from the interacting V states to superexcited Rydberg states by autoionization (HI^+), photodissociation (H^+) and photoionization (H^+ and I^+) (Fig. 8(a)). Furthermore, HI^+ and I^+ are formed via direct one-photon excitations of the $j(v' = 0)$ Rydberg state to a superexcited Rydberg state by autoionization (HI^+) and photodissociation (H^+). The $k(v' = 2)$ state, which, on the other hand, experiences weak heterogeneous interactions with the $V(v' = m + 13)$ ion-pair state for $J' = 10$ -11 and the $j(0)$ state for $J' = 8 - 9$, therefore, will form the ions H^+, I^+ and HI^+ via one-photon excitations from the mixed $V(v' = m + 13)$ state for $J' = 8 - 11$ only, but I^+ and HI^+ via direct excitations of the $k(v' = 2)$ Rydberg state for all J's (Fig. 8(b)).

Despite the limitations of the standard REMPI technique in terms of detecting photofragments without vector alignments as in e.g. velocity map imaging, this study extends the applicability of the REMPI technique to involve the study of photofragmentation pathways which involve Rydberg and ion-par states as intermediates beyond its more common use for spectra recording and analysis. Imaging the individual photofragments of the $j(0)$ vs $k(2)$ system would still bring invaluable insights into the mechanisms that govern photofragmentations in the energy gap of concern.

ACKNOWLEDGMENTS

The financial support of the University Research Fund, University of Iceland and the Icelandic Science Foundation (Grant No. 130259-051) is gratefully acknowledged. We would also like to than Huasheng Wang for useful help with the experiments.

Figure captions

Fig. 1. REMPI spectra of HI for the ions H^+, I^+, and HI^+. *J*-quantum numbers for the excited states (J') of rotational peaks corresponding to two-photon resonance excitations from the ground state to the $j^3\Sigma^-(0^+; v' = 0)$ and $k^3\Pi_1(v' = 2)$ Rydberg states are indicated. *Q* lines due to transitions to a $^3\Sigma^-(\Omega = 1)$ Rydberg state are marked. An iodine atomic line, at 73 117.9 cm^{-1}, is marked.

Fig.2. Potential energy curves and quantum energy levels for the $j^3\Sigma^-(0^+; v' = 0)$ and $k^3\Pi_1(v' = 2)$ Rydberg states. The rotational energies levels were derived from the REMPI spectra (Fig. 1). Near-degenerate interactions between levels $J' = 9$ and 10 are indicated. The potential curve for the $k^3\Pi_1(v' = 2)$ state was derived from available spectroscopic constants.[4, 55, 57] The

shape of the potential curve for the $j^3\Sigma^-(0^+;\ v' = 0)$ state was approximated by the curve for the $k^3\Pi_1(v' = 2)$ state.

Fig. 3. (a) Spacing between rotational levels ($\Delta E_{J',\ J'-1}$) as a function of J'; experimental values (dots) and fit curves for the $j^3\Sigma^-(0^+;\ v' = 0)$ and $k^3\Pi_1(v' = 2)$ states and (b) the corresponding reduced term value plots.

Fig. 4 (a) Total relative rotational line intensities of the $j^3\Sigma^-(0^+;\ v' = 0)$ (blue) and $k^3\Pi_1(v' = 2)$ (red) spectra as a function of J'. (b) Observed total intensity ratios of the Q lines for the $k^3\Pi_1(v' = 2)$ and $j^3\Sigma^-(0^+;\ v' = 0)$ spectra ($I(k(2))/I(j(0))$) (black) as a function of J' and calculated intensity ratios for non-interacting states derived by fitting the data points for $J' = 2$ - 5 by the expression on the right side of Eq. (11b) for μ_0^2, μ_2^2 and $K(k)/K(j)$ as variables.

Fig. 5 (a) Relative H^+ ion signal intensities ($I(H^+)/I_{total}$) vs J' derived from the Q rotational lines of the $j^3\Sigma^-(0^+;\ v' = 0)$ and $k^3\Pi_1(v' = 2)$ spectra. (b) Relative ion signal intensities ($I(M^+)/I_{total}$), $M^+ = I^+$, HI^+ vs J' derived from the Q rotational lines of the $j^3\Sigma^-(0^+;\ v' = 0)$ spectrum.

Fig. 6 (a) Rotational linewidths as a function of J' derived from the Q lines of the H^+, I^+, and HI^+ signals for the (a) $j^3\Sigma^-(0^+;\ v' = 0)$ and (b) $k^3\Pi_1(v' = 2)$ spectra.

Fig. 7 Potential energy curves, asymptotic energies and photon excitations relevant to state interactions and photofragmentation processes of the $j^3\Sigma^-(0^+;\ v' = 0)$ and $k^3\Pi_1(v' = 2)$ states as discussed in the paper. The potential curves of the $X^2\Pi$, $A^2\Sigma^+$, $[A^2\Sigma^+]5d\pi$ and the repulsive states are derived from references [38], [27], [47] and [21] respectively. For the purpose of this paper,

the potential curve of the $V^1\Sigma^+$ ion-pair state was fitted arbitrarily to encompass the lowest observed vibrational state, namely $V(m)$.[4] Arrows shown correspond to single photon 36 607.6 cm^{-1} excitations.

Fig. 8 Schematic figures summarizing state interactions (near- and non- degenerate interactions), photoexcitation and photofragmentation (photodissociation, autoionization, photoionization) processes involved (see main text) with respect to the (a) $j^3\Sigma_u^-(0_u^+;\ v' = 0)$ and (b) $k^3\Pi_1(v' = 2)$ Rydberg states. Formed ions are highlighted by circles

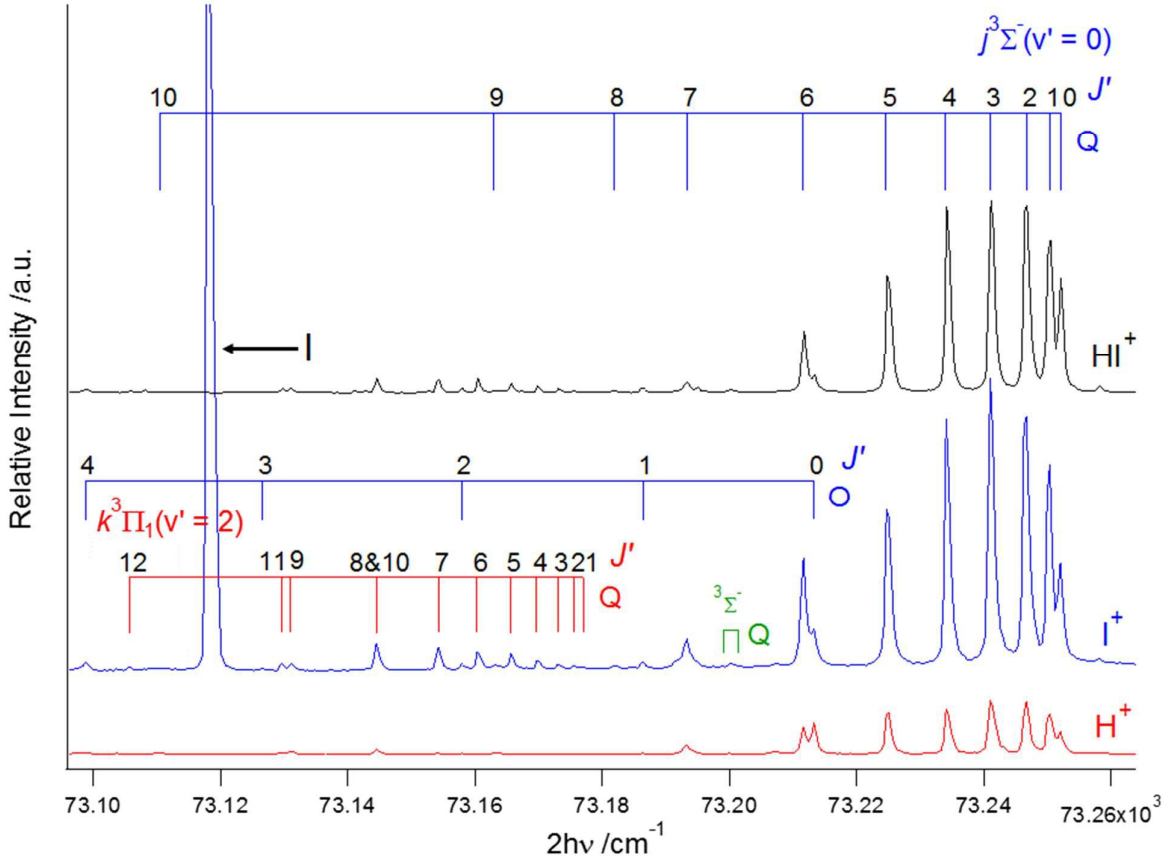

Fig. 1

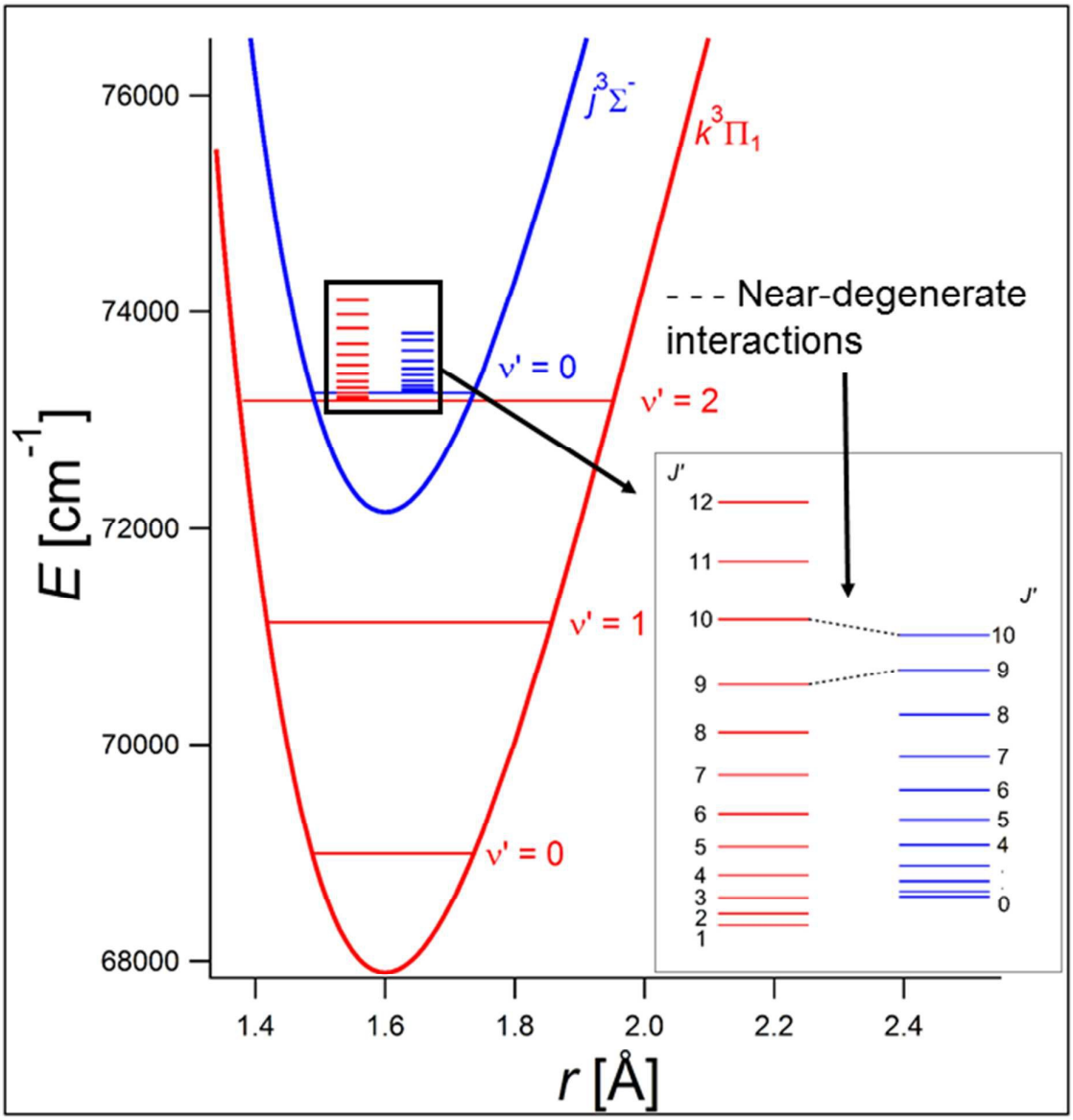

Fig. 2

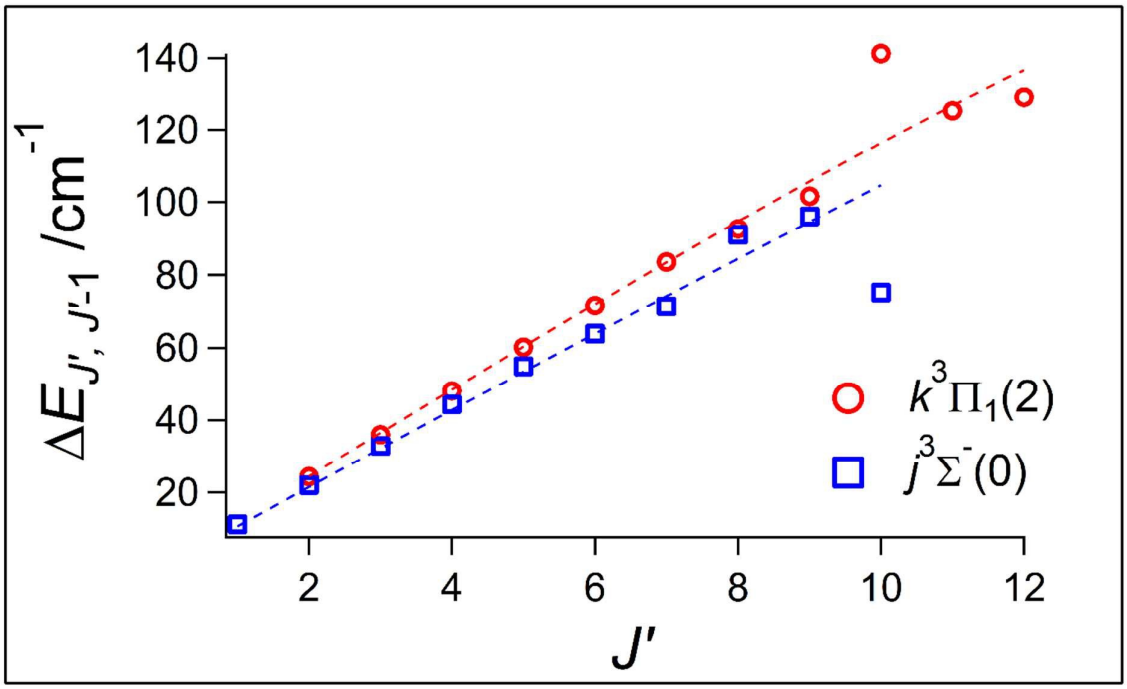

Fig. 3a

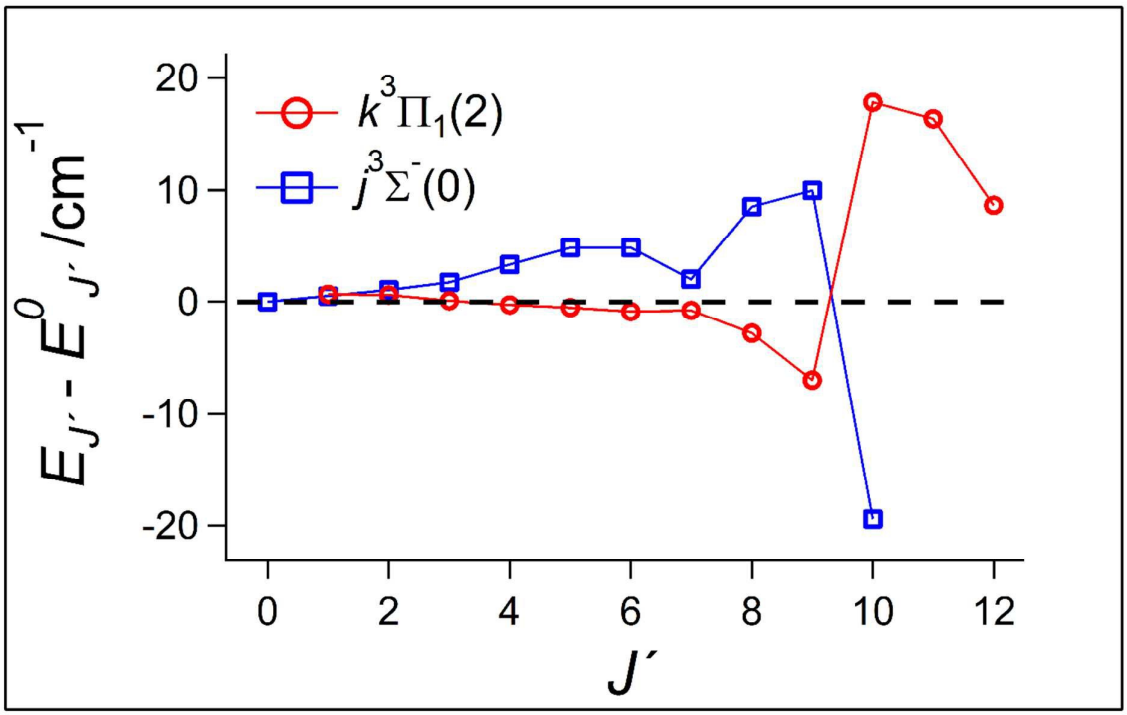

Fig. 3b

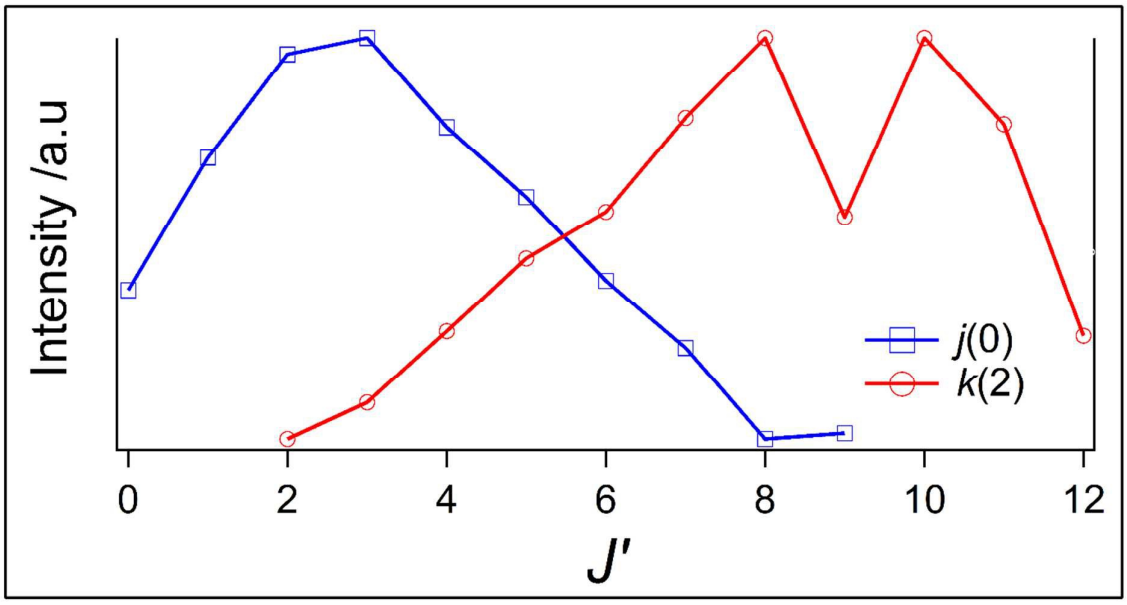

Fig. 4a

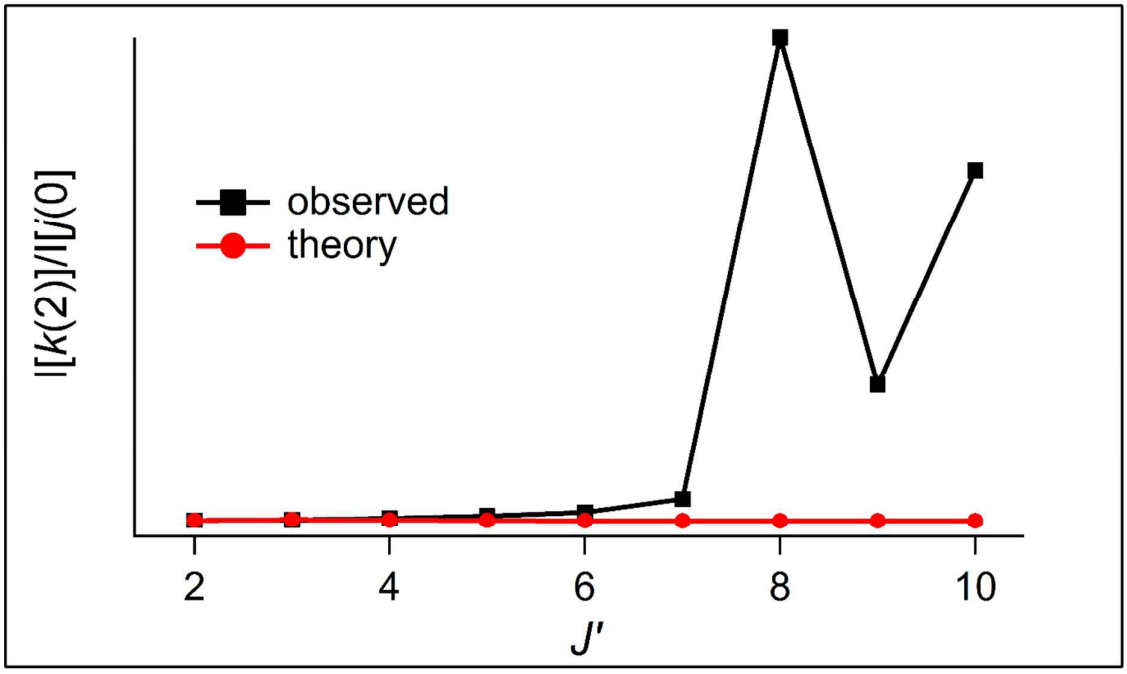

Fig. 4b

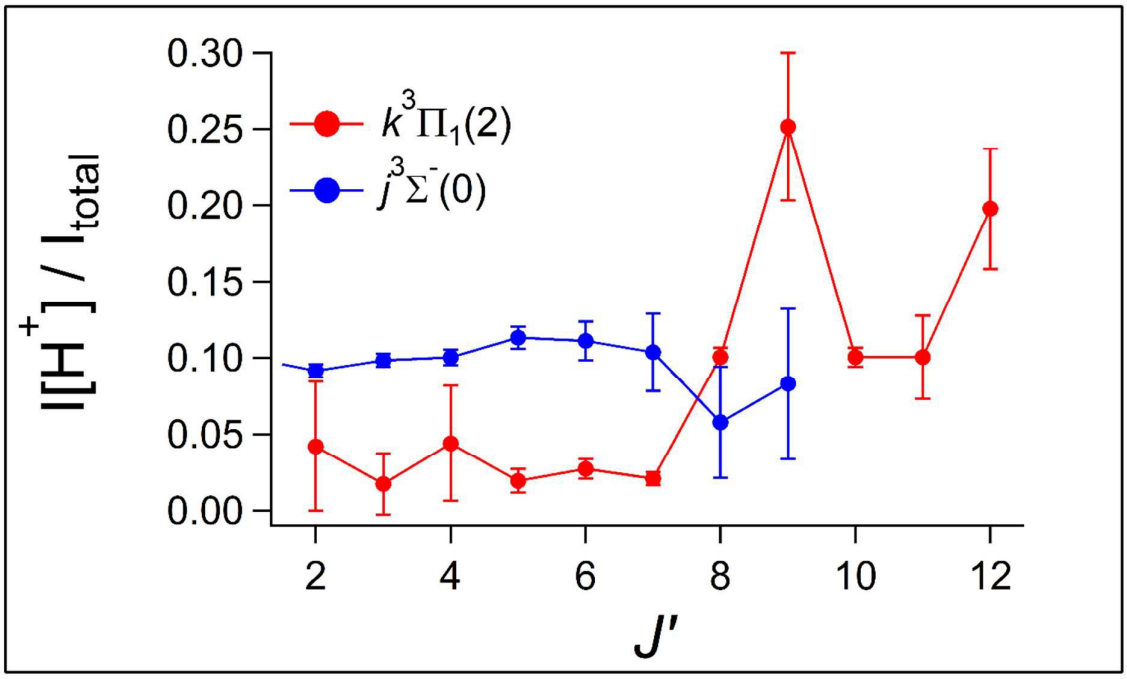

Fig. 5a

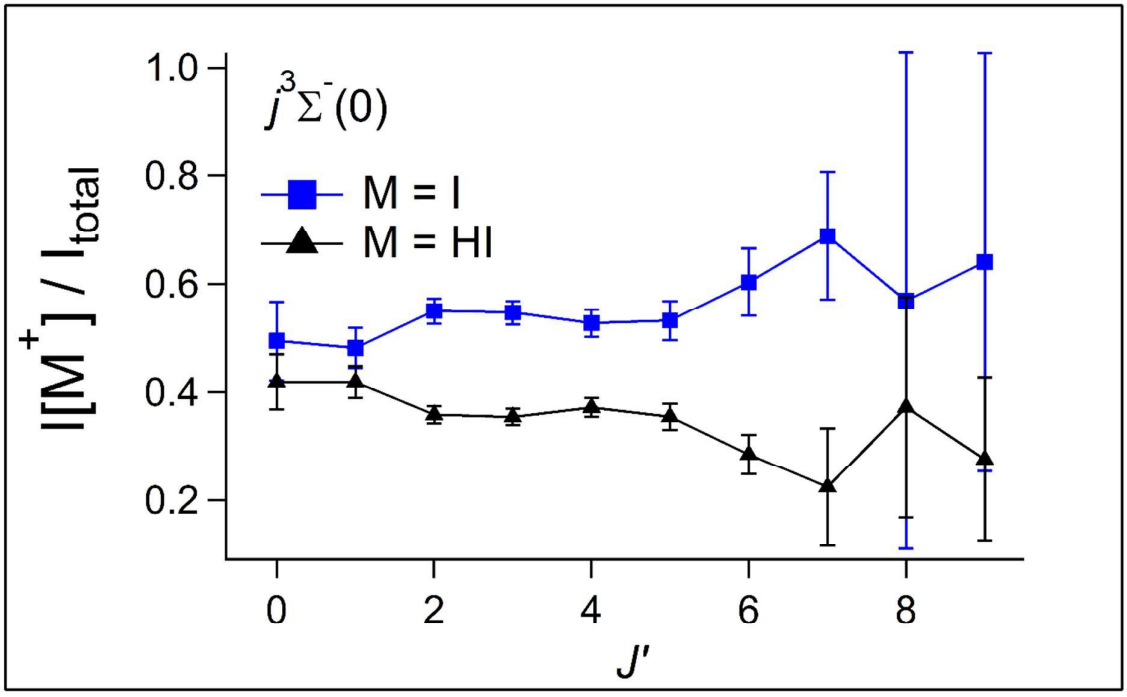

Fig. 5b

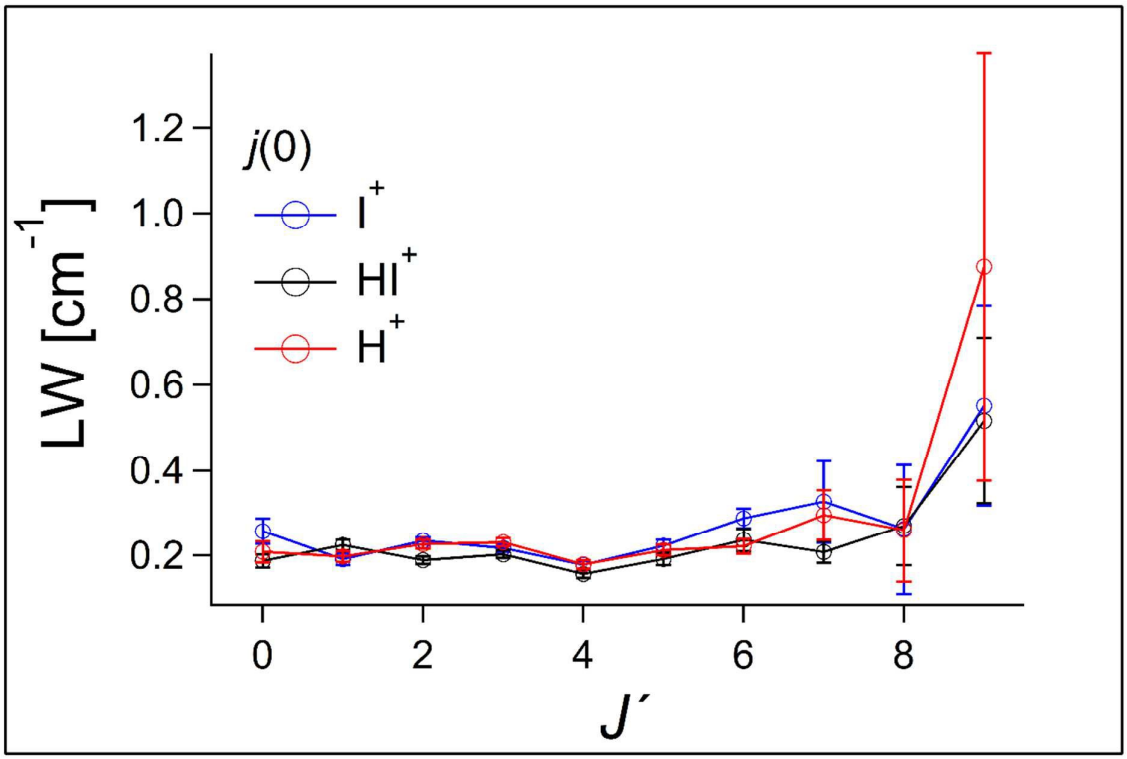

Fig. 6a

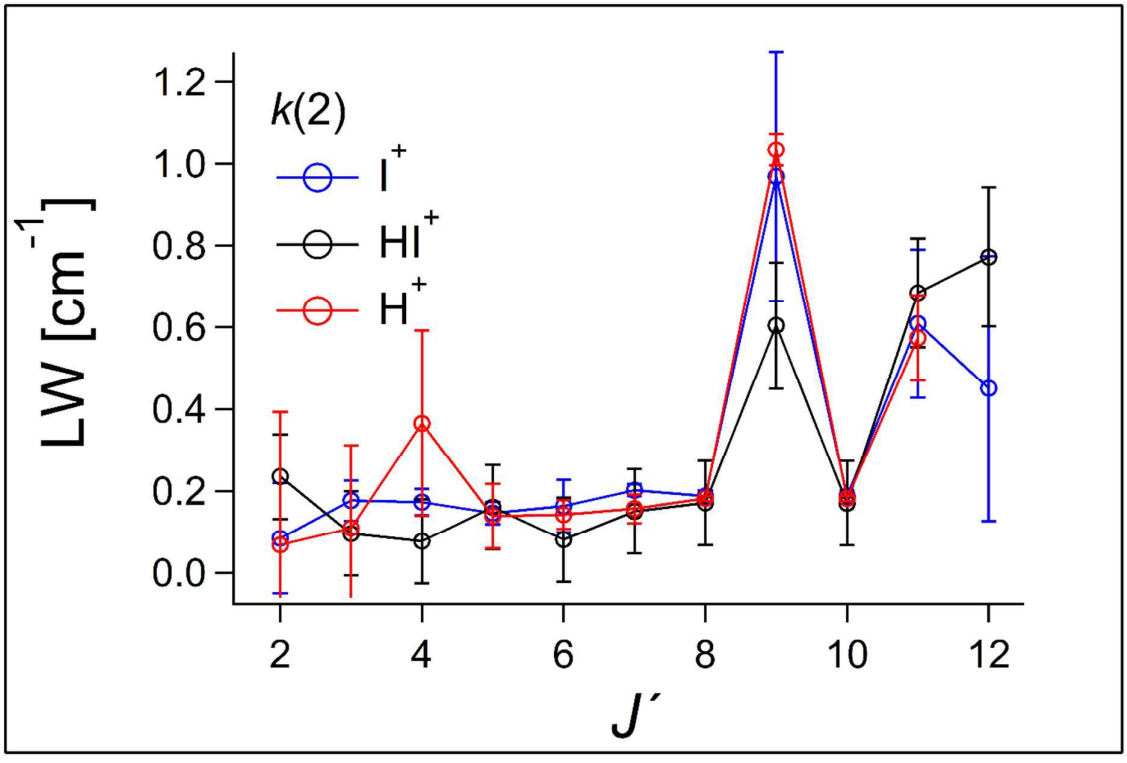

Fig. 6b

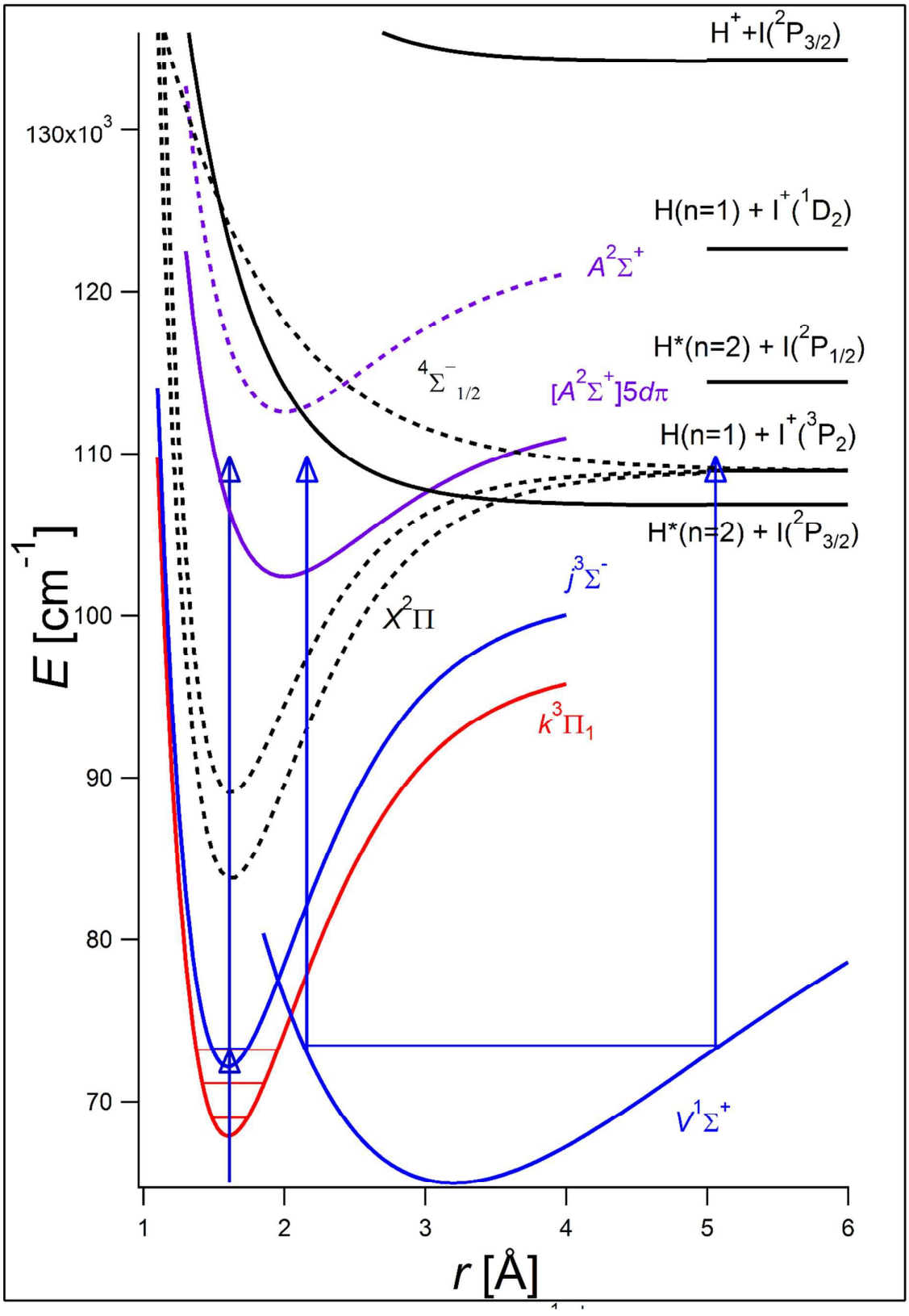

Fig. 7

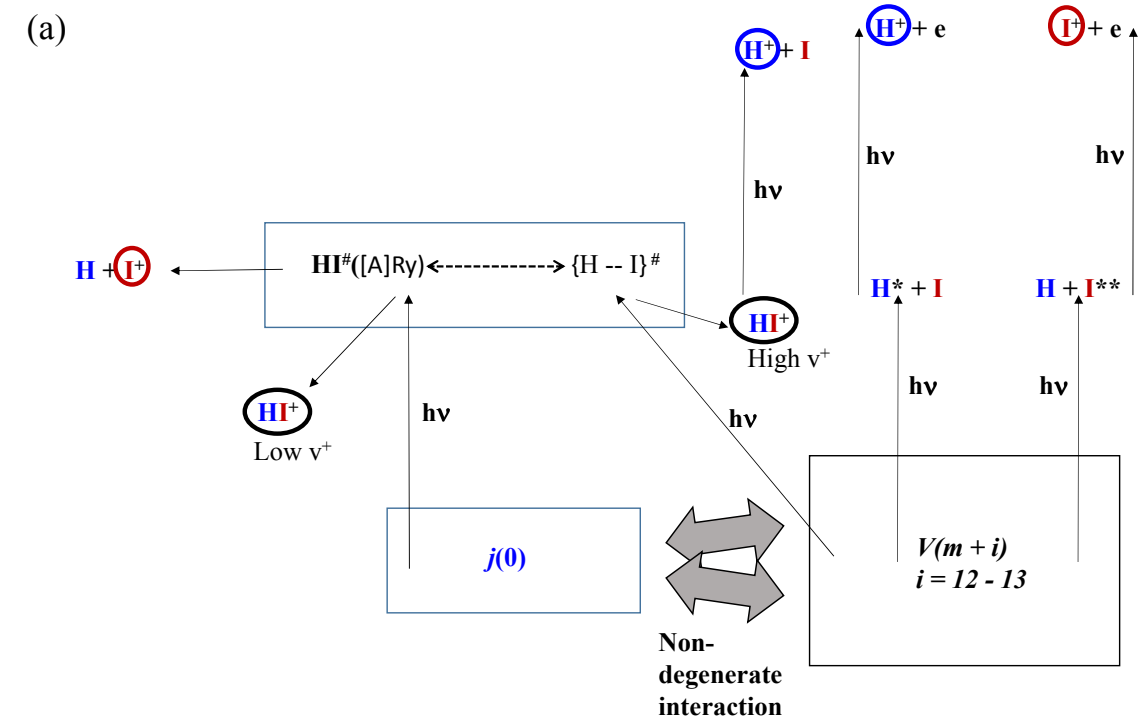

Fig. 8 a

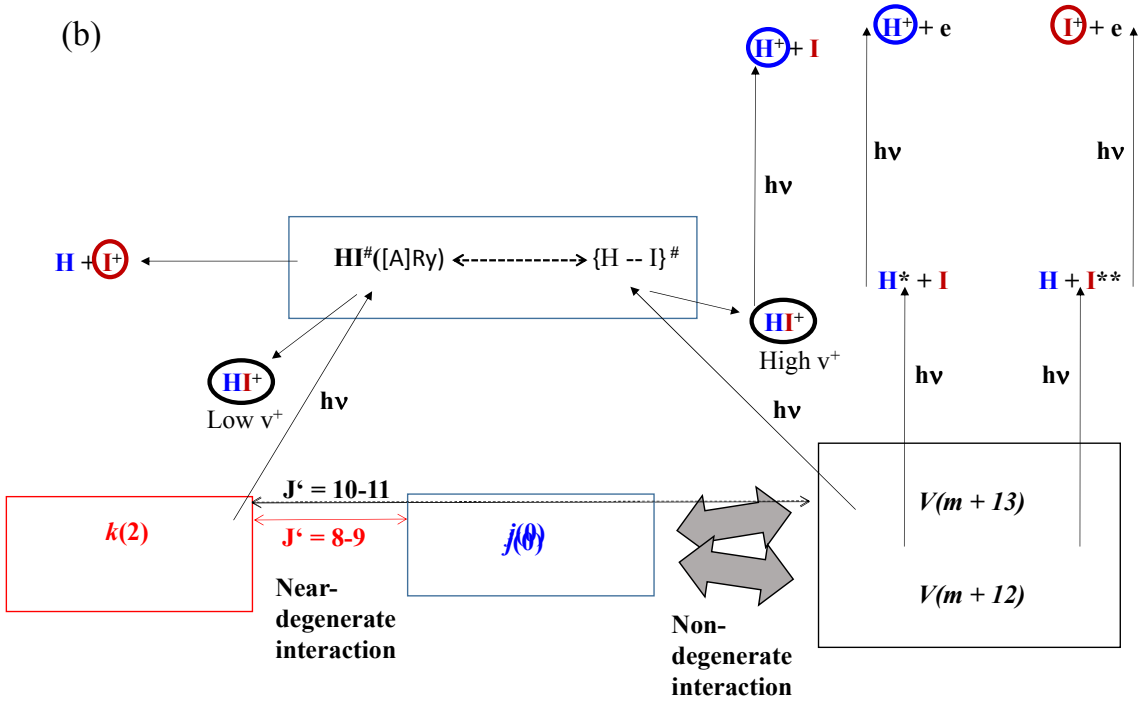

Fig. 8 b

Tables

Table 1 Rotational lines for HI due to two-photon resonance transitions (cm^{-1}) from the ground state ($X^1\Sigma^+(v'' = 0)$ to the $j^3\Sigma^-(0^+; v' = 0)$ and $k^3\Pi_1(v' = 2)$ Rydberg states vs. *J*-quantum numbers for the upper states (*J′*).

	$k^3\Pi_1(2)$	$j^3\Sigma^-(0^+; 0)$		
J′	*Q*	*O*	*Q*	*S*
0		73213.3	73252.0	
1	73177.0	73186.4	73250.4	
2	73175.6	73157.9	73246.7	73285.8
3	73173.0	73126.6	73241.0	73309.1
4	73169.7	73098.4	73234.0	73328.7
5	73165.6		73224.7	73345.4
6	73160.3		73211.6	
7	73154.2		73193.3	
8	73144.5		73181.9	
9	73131.0		73105.7	
10	73144.5		73056.6	
11	73129.5			
12	73105.7			

Table 2. Parameter values (cm^{-1}; level energies (E), energy level differences ($\Delta E_{J'}$) and interaction strengths (W_{12}') relevant to near-degenerate interactions between the $j^3\Sigma^-(0^+;\ v' = 0)$ and $k^3\Pi_1(v' = 2)$ Rydberg states for $J' = 9$ and 10, derived from perturbation analysis based on peak positions (see text).

J'	E / $k(2)$ state	E / $j(0)$ state	ΔE	$\langle W_{12}' \rangle$
9	73707.7	73739.6	-31.9	1.52 ± 0.09
10	73848.9	73814.8	34.1	

Table 3. Spectroscopic parameters (cm^{-1}) for the $k^3\Pi_1(v' = 2)$ and $j^3\Sigma^-(0^+;\ v' = 0)$ Rydberg states derived from our REMPI spectra and from reported work by Ginter et al. [4]

	$k^3\Pi_1(v' = 2)$		$j^3\Sigma^-(0^+;\ v' = 0)$	
	This work	Others[4]	This work	Others[4]
v^0	73180.0	73180.7	73252.0	73254.9
$B_{v'}$	6.10 ± 0.06	6.034	5.37 ± 0.06	5.706
$D_{v'}$	0.0014 ± 0.0005	0.000872	0.0007 ± 0.0007	0.00475

References

1. W. C. Price, *Proc. Roy. Soc. Ser. A*, 1938, 167, 216.
2. S. G. Tilford, M. L. Ginter and A. M. Bass, *J. Mol. Spectrosc.*, 1970, 34, 327.
3. M. L. Ginter, S. G. Tilford and A. M. Bass, *J. Mol. Spectrosc.*, 1975, 57, 271.
4. D. S. Ginter, M. L. Ginter and S. G. Tilford, *J. Mol. Spectrosc.*, 1982, 92, 40.
5. H. T. Wang, W. S. Felps, G. L. Findley, A. R. P. Rau and S. P. McGlynn, *J. Chem. Phys.*, 1977, 67, 3940-3946.
6. R. S. Mulliken, *Phys. Rev.* , 1937, 51, 310.
7. J. F. Ogilvie, *Transactions of the Faraday Society*, 1971, 67, 2205.
8. R. D. Clear, S. J. Riley and K. R. Wilson, *J. Chem. Phys.*, 1975, 63, 1340-1347.
9. R. Schmiedl, H. Dugan, W. Meier and K. H. Welge, *Z. Phys. A.-Hadrons Nuclei*, 1982, 304, 137-142.
10. P. Brewer, P. Das, G. Ondrey and R. Bersohn, *J. Chem. Phys.*, 1983, 79, 720-723.
11. G. N. A. van Veen, K. A. Mohamed, T. Baller and A. E. Devries, *Chemical Physics*, 1983, 80, 113-120.
12. I. Levy and M. Shapiro, *J. Chem. Phys.*, 1988, 89, 2900-2908.
13. Z. Xu, B. Koplitz and C. Wittig, *J. Chem. Phys.*, 1989, 90, 2692-2702.
14. T. N. Kitsopoulos, M. A. Buntine, D. P. Baldwin, R. N. Zare and D. W. Chandler, *SPIE*, 1993, 1858, 2.
15. V. Kleiman, L. C. Zhu, X. N. Li and R. J. Gordon, *Abstr. Pap. Am. Chem. Soc.*, 1995, 210, 238-PHYS.
16. L. C. Zhu, V. Kleiman, X. N. Li, S. P. Lu, K. Trentelman and R. J. Gordon, *Science*, 1995, 270, 77-80.
17. L. Zhu, K. Suto, J. A. Fiss, R. Wada, T. Seideman and R. J. Gordon, *Phys. Rev. Lett.*, 1997, 79, 4108-4111.
18. J. A. Fiss, L. C. Zhu, K. Suto, G. Z. He and R. J. Gordon, *Chemical Physics*, 1998, 233, 335-341.
19. S. R. Langford, P. M. Regan, A. J. Orr-Ewing and M. N. R. Ashfold, *Chemical Physics*, 1998, 231, 245-260.
20. P. M. Regan, D. Ascenzi, C. Clementi, M. N. R. Ashfold and A. J. Orr-Ewing, *Chem. Phys. Lett.*, 1999, 315, 187-193.
21. S. Manzhos, H. P. Loock, B. L. G. Bakker and D. H. Parker, *J. Chem. Phys.*, 2002, 117, 9347-9352.

22. J. P. Camden, H. A. Bechtel, D. J. A. Brown, A. E. Pomerantz, R. N. Zare and R. J. Le Roy, *J. Phys. Chem. A*, 2004, 108, 7806-7813.
23. S. R. Ungemach, H. F. Schaefer and B. Liu, *Journal of Molecular Spectroscopy*, 1977, 66, 99-105.
24. H. Lefebvre-Brion, A. Giustisuzor and G. Raseev, *J. Chem. Phys.*, 1985, 83, 1557-1566.
25. A. Mank, M. Drescher, T. Huthfehre, N. Böwering, U. Heinzmann and H. Lefebvre-Brion, *J. Chem. Phys.*, 1991, 95, 1676-1687.
26. R. J. Le Roy, G. T. Kraemer and S. Manzhos, *J. Chem. Phys.*, 2002, 117, 9353-9369.
27. A. J. Yencha, P. Baltzer, A. J. Cormack, Y. Li, H. P. Liebermann, A. B. Alekseyev and R. J. Buenker, *J. Chem. Phys.*, 2003, 119, 5943-5948.
28. A. Brown, *J. Chem. Phys.*, 2005, 122, 12.
29. D. N. Jodoin and A. Brown, *J. Chem. Phys.*, 2005, 123, 10.
30. A. Brown, *Int. J. Quantum Chem.*, 2007, 107, 2665-2671.
31. J. H. D. Eland and J. Berkowitz, *J. Chem. Phys.*, 1977, 67, 5034-5039.
32. T. A. Carlson, P. Gerard, M. O. Krause, G. Vonwald, J. W. Taylor and F. A. Grimm, *J. Chem. Phys.*, 1986, 84, 4755-4759.
33. D. J. Hart and J. W. Hepburn, *Chemical Physics*, 1989, 129, 51-64.
34. H. J. Lempka, T. R. Passmore and W. C. Price, *Proc. R. Soc. London Ser. A*, 1968, 304, 53.
35. N. Böwering, M. Muller, M. Salzmann and U. Heinzmann, *J. Phys. B-At. Mol. Opt. Phys.*, 1991, 24, 4793-4801.
36. N. Böwering, H. W. Klausing, M. Muller, M. Salzmann and U. Heinzmann, *Chem. Phys. Lett.*, 1992, 189, 467-472.
37. N. Böwering, M. Salzmann, M. Muller, H. W. Klausing and U. Heinzmann, *Phys. Rev. A*, 1992, 45, R11-R14.
38. C. J. Zietkiewicz, Y. Y. Gu, A. M. Farkas and J. G. Eden, *J. Chem. Phys.*, 1994, 101, 86-94.
39. A. J. Yencha, M. W. Ruf and H. Hotop, *Z. Phys. D-Atoms Mol. Clusters*, 1994, 29, 163-177.
40. A. Chanda, W. C. Ho and I. Ozier, *J. Chem. Phys.*, 1995, 102, 8725-8735.
41. A. J. Cormack, A. J. Yencha, R. J. Donovan, K. P. Lawley, A. Hopkirk and G. C. King, *Chemical Physics*, 1997, 221, 175-188.
42. D. J. Gendron and J. W. Hepburn, *J. Chem. Phys.*, 1998, 109, 7205-7213.

43. S. A. Wright and J. D. McDonald, *J. Chem. Phys.*, 1994, 101, 238-245.
44. S. T. Pratt and M. L. Ginter, *J. Chem. Phys.*, 1995, 102, 1882-1888.
45. P. M. Regan, D. Ascenzi, E. Wrede, P. A. Cook, M. N. R. Ashfold and A. J. Orr-Ewing, *Phys. Chem. Chem. Phys.*, 2000, 2, 5364-5374.
46. H. P. Loock, B. L. G. Bakker and D. H. Parker, *Can. J. Phys.*, 2001, 79, 211-227.
47. Y. Hikosaka and K. Mitsuke, *J. Chem. Phys.*, 2004, 121, 792-799.
48. Á. Kvaran, H. S. Wang, K. Matthiasson, A. Bodi and E. Jonsson, *J. Chem. Phys.*, 2008, 129, 164313.
49. Á. Kvaran, K. Matthiasson and H. S. Wang, *J. Chem. Phys.*, 2009, 131, 044324.
50. K. Matthiasson, J. M. Long, H. S. Wang and Á. Kvaran, *J. Chem. Phys.*, 2011, 134, 164302.
51. J. Long, H. Wang and Á. Kvaran, *J. Chem. Phys.*, 2013, 138, 044308.
52. J. Long, H. R. Hrodmarsson, H.Wang and Á. Kvaran, *J. Chem. Phys.*, 2012, 136, 214315.
53. H. R. Hrodmarsson, H. S. Wang and A. Kvaran, *Journal of Molecular Spectroscopy*, 2013, 290, 5-12.
54. H. R. Hrodmarsson, H. S. Wang and Á. Kvaran, *J. Chem. Phys.*, 2014, 140, 10.
55. H. R. Hrodmarsson, H. S. Wang and Á. Kvaran, *J. Chem. Phys.*, 2015, 142, 244312.
56. J. Long, H. Wang and Á. Kvaran, *J. Mol. Spectrosc.*, 2012, 282, 20-26.
57. H. R. Hrodmarsson, H. S. Wang and Á. Kvaran, *J. Mol. Spectros.*, 2013, 290, 5-12.
58. H. Lefebvre-Brion and R. W. Field, *The Spectra and Dynamics of Diatomic Molecules*, Elsevier, Amsterdam, 2004.
59. P. A. M. Dirac, *The Principles of Quantum Mechanics*, Oxford University Press, 1930.
60. R. G. Bray and R. M. Hochstrasser, *Molecular Physics*, 1976, 31, 1199-1211.
61. R. J. Donovan, in *Gas Kinetics and Energy Transfer*, eds. P. G. Ashmore and R. J. Donovan, The Royal Society of Chemistry, London, 1981, vol. 4, pp. 117-136.
62. Á. Kvaran, H. Wang and Á. Logadóttir, in *Recent Res. Devel. in Physical Chem.*, Transworld Research Network, 1998, vol. 2, pp. 233-244.
63. J. B. Halpern, H. Zacharias and R. Wallenstein, *J. Mol. Spectrosc.*, 1980, 79, 1-30.
64. R. N. Zare, *Angular Momentum - Understanding Spatial Aspects in Chemistry and Physics*, John Wiley and Sons Inc., USA, 1988.
65. Á. Kvaran, Á. Logadóttir and H. Wang, *J. Chem. Phys.*, 1998, 109, 5856-5867.

66. D. S. Ginter, M. L. Ginter, S. G. Tilford and A. M. Bass, *J. Mol. Spectrosc.*, 1982, 92, 55.
67. C. M. Western, University of Bristol,, University of Bristol,.
68. E. Luc-Koenig and C. V. Morillon, J, *Phys. Scr.*, 1975, 12, 199-219.
69. D. S. Green, G. A. Bickel and S. C. Wallace, *J. Mol. Spectrosc.*, 1991, 150, 303-353.
70. D. S. Green, G. A. Bickel and S. C. Wallace, *J. Mol. Spectrosc.*, 1991, 150, 354-387.
71. D. S. Green, G. A. Bickel and S. C. Wallace, *J. Mol. Spectrosc.*, 1991, 150, 388-469.
72. D. S. Green and S. C. Wallace, *J. Chem. Phys.*, 1992, 96, 5857-5877.
73. Á. Kvaran, H. Wang and B. G. Waage, *Can. J. Physics*, 2001, 79, 197-210.
74. A. I. Chichinin, C. Maul and K.-H. Gericke, *J. Chem. Phys.*, 2006, 124, 224324.
75. A. I. Chichinin, P. S. Shternin, N. Gödecke, S. Kauczok, C. Maul, O. S. Vasyutinskii and K.-H. Gericke, *J. Chem. Phys.*, 2006, 125, 034310.
76. C. Romanescu and H. P. Loock, *J. Chem. Phys.*, 2007, 127, 13.
77. A. I. Chichinin, K.-H. Gericke, S. Kauczok and C. Maul, *International Reviews in Physical Chemistry*, 2009, 28, 607-680.
78. C. Romanescu and H. P. Loock, *Phys. Chem. Chem. Phys.*, 2006, 8, 2940-2949.
79. D. Zaouris, A. Kartakoullis, P. Glodic, P. C. Samartzis, H. R. Hrodmarsson and Á. Kvaran, *Phys. Chem. Chem. Phys.*, 2015, DOI: 10.1039/C5CP00748H.
80. C. Romanescu, S. Manzhos, D. Boldovsky, J. Clarke and H. Loock, *J. Chem. Phys*, 2004, 120, 767-777.
81. S. Kauczok, C. Maul, A. I. Chichinin and K. H. Gericke, *J. Chem. Phys.*, 2010, 133, 10.
82. M. H. Alexander, X. N. Li, R. Liyanage and R. J. Gordon, *Chem. Phys.*, 1998, 231, 331-343.